iScience

CellPress
OPEN ACCESS

Article

# Norepinephrine modulates wakefulness via α1 adrenoceptors in paraventricular thalamic nucleus

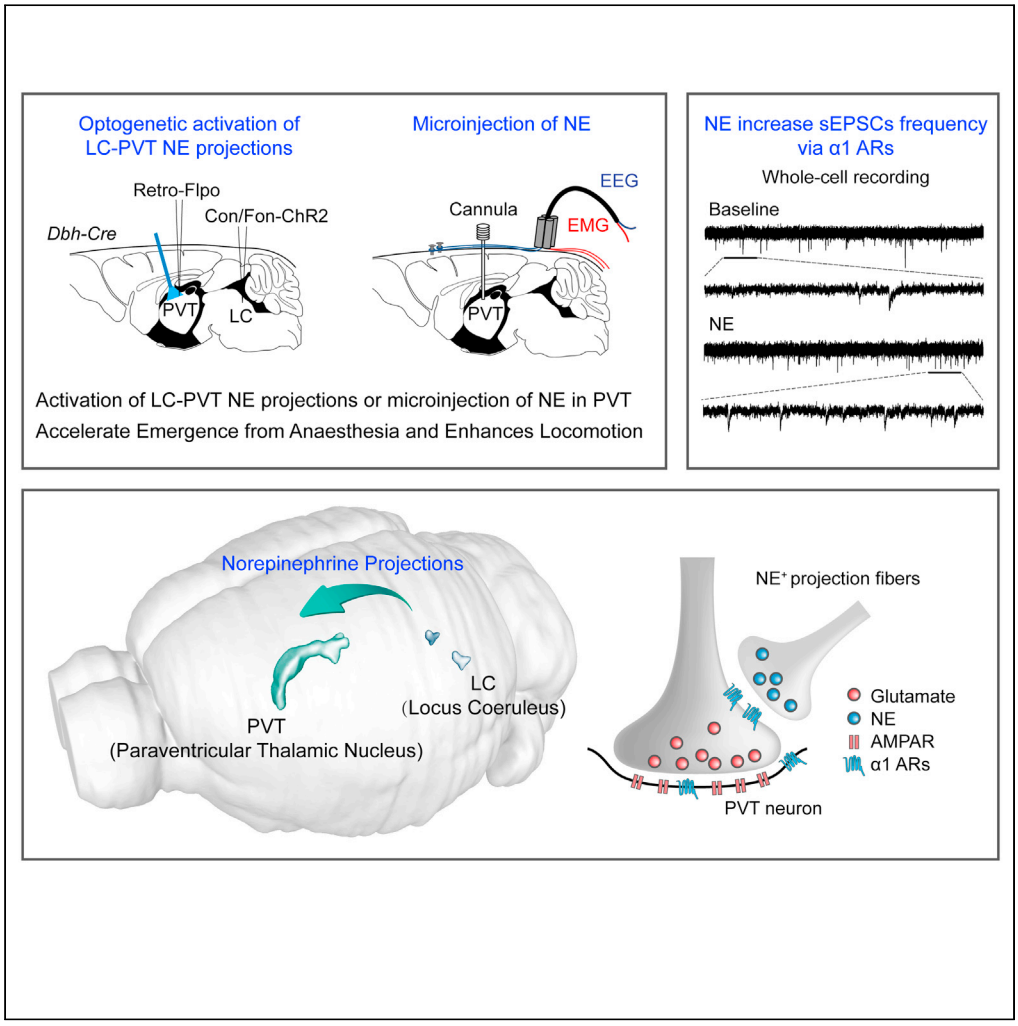


Yan Wang, Ling Xu, Ming-Zhe Liu, ..., Ling Zhang, Li-Na Huang, Di Mu

lina.huang@shgh.cn (L.-N.H.)
damonmu@163.com, 018501md@shgh.cn (D.M.)

## Highlights

The PVT-projecting LC NE⁺ neurons had few collateral projections to other brain nuclei

NE in the PVT accelerated emergence from anesthesia and enhanced locomotion activity

NE increased the activity of the PVT neurons via α1 adrenoceptors

Wang et al., iScience 24, 103015
September 24, 2021 
https://doi.org/10.1016/j.isci.2021.103015

iScience

CellPress
OPEN ACCESS

Article

# Norepinephrine modulates wakefulness via α1 adrenoceptors in paraventricular thalamic nucleus

Yan Wang,[1,6] Ling Xu,[1,6] Ming-Zhe Liu,[2,6] Dan-Dan Hu,[3] Fang Fang,[4] Dao-Jie Xu,[5] Rui Zhang,[1] Xiao-Xiao Hua,[3] Jin-Bao Li,[1] Ling Zhang,[3] Li-Na Huang,[1,*] and Di Mu[1,7,*]

## SUMMARY

**Norepinephrine (NE) neurons in the locus coeruleus (LC) play key roles in modulating sleep and wakefulness. Recent studies have revealed that the paraventricular thalamic nucleus (PVT) is a critical wakefulness-controlling nucleus in mice. However, the effects of NE on PVT neurons remain largely unknown. Here, we investigated the mechanisms of NE modulating wakefulness in the PVT by using viral tracing, behavioral tests, slice electrophysiology, and optogenetics techniques. We found that the PVT-projecting LC neurons had few collateral projections to other brain nuclei. Behavioral tests showed that specific activation of the LC-PVT projections or microinjection of NE into the PVT accelerated emergence from general anesthesia and enhanced locomotion activity. Moreover, brain slice recording results indicated that NE increased the activity of the PVT neurons mainly by increasing the frequency of spontaneous excitatory postsynaptic currents via α1 adrenoceptors. Thus, our results demonstrate that NE modulates wakefulness via α1 adrenoceptors in the PVT.**

## INTRODUCTION

Previous studies have provided a framework for understanding the neural circuitry of wakefulness and sleep, which is of great scientific interest and clinical importance (Adamantidis et al., 2019; Scammell et al., 2017; Weber and Dan, 2016). A recent study reported that the paraventricular thalamic nucleus (PVT) is a critical node for controlling wakefulness in rodents (Ren et al., 2018). Activation of PVT neurons induces a transition from sleep to wakefulness as well as the acceleration of emergence from isoflurane-induced anesthesia (Ren et al., 2018). The PVT receives a diverse array of afferents from the cortex, hypothalamus, and brainstem, including the locus coeruleus (LC) (Szabadi, 2013; Vertes et al., 2015). The LC norepinephrine (NE) system has a broad projection throughout the brain (Chandler et al., 2019). The LC and its neuromodulator NE (also known as noradrenaline) are important for promoting arousal (Breton-Provencher and Sur, 2019; Carter et al., 2010; Hayat et al., 2020; Vazey and Aston-Jones, 2014) and a subpart of this system promotes sedation and hypothermia through α2 adrenoceptors (Zhang et al., 2015). However, whether LC-PVT projection modulates wakefulness is still unknown.

NE is known to have complex effects on modulating membrane potential (Grzelka et al., 2017), cellular excitability (Church et al., 2019), and synaptic plasticity (Barresi et al., 2014; Gu, 2002) in different brain areas through three major categories of adrenoceptors (ARs): α1 (Gq-coupled receptors, including α1A, α1B, and α1D), α2 (Gi-coupled receptors, including α2A, α2B, and α2C) and β (Gs-coupled receptors, including β1 and β2) (Sara, 2009). Multiple AR subtypes are expressed in the PVT neurons, including α1B (Pieribone et al., 1994), α2C (Rosin et al., 1996), β1, and β2 ARs (Rainbow et al., 1984). Notably, a recent study reported that PVT-projecting fibers co-release dopamine and reduce inhibitory transmission onto PVT neurons by postsynaptic dopamine receptor 2 (D2R) (Beas et al., 2018). Another study also showed that NE could activate D2R nonspecifically and modulate the neurons' activities in other brain regions (Arencibia-Albite et al., 2007). The ARs mechanisms of NE's effect in the PVT require further investigation.

Given the importance of the PVT in controlling wakefulness and the lack of direct exploration of NE's effects on PVT neurons, we performed virus tracing and found that the PVT-projecting LC neurons had few collateral projections to other nuclei. Specific activation of the LC-PVT projections or microinjection of NE into the PVT accelerated emergence from general anesthesia and enhanced locomotion. Furthermore, whole-cell recording results on acute brain slices confirmed that NE depolarized PVT neurons by enhancing the

[1]Department of Anesthesiology, Shanghai General Hospital, Shanghai Jiao Tong University School of Medicine, No. 650 Xin Song Jiang Road, Shanghai 201620, China

[2]Department of Respiratory, The First Affiliated Hospital of Guangzhou Medical University, Guangzhou 510120, China

[3]Tongji University School of Medicine, Shanghai, China

[4]Department of Endocrinology, Shanghai General Hospital, Shanghai Jiao Tong University School of Medicine, Shanghai 201620, China

[5]Department of Anesthesiology, Huashan Hospital, Fudan University, Shanghai 200040, China

[6]These authors contributed equally

[7]Lead contact

*Correspondence: lina.huang@shgh.cn (L.-N.H.), damonmu@163.com, 018501md@shgh.cn (D.M.)

https://doi.org/10.1016/j.isci.2021.103015

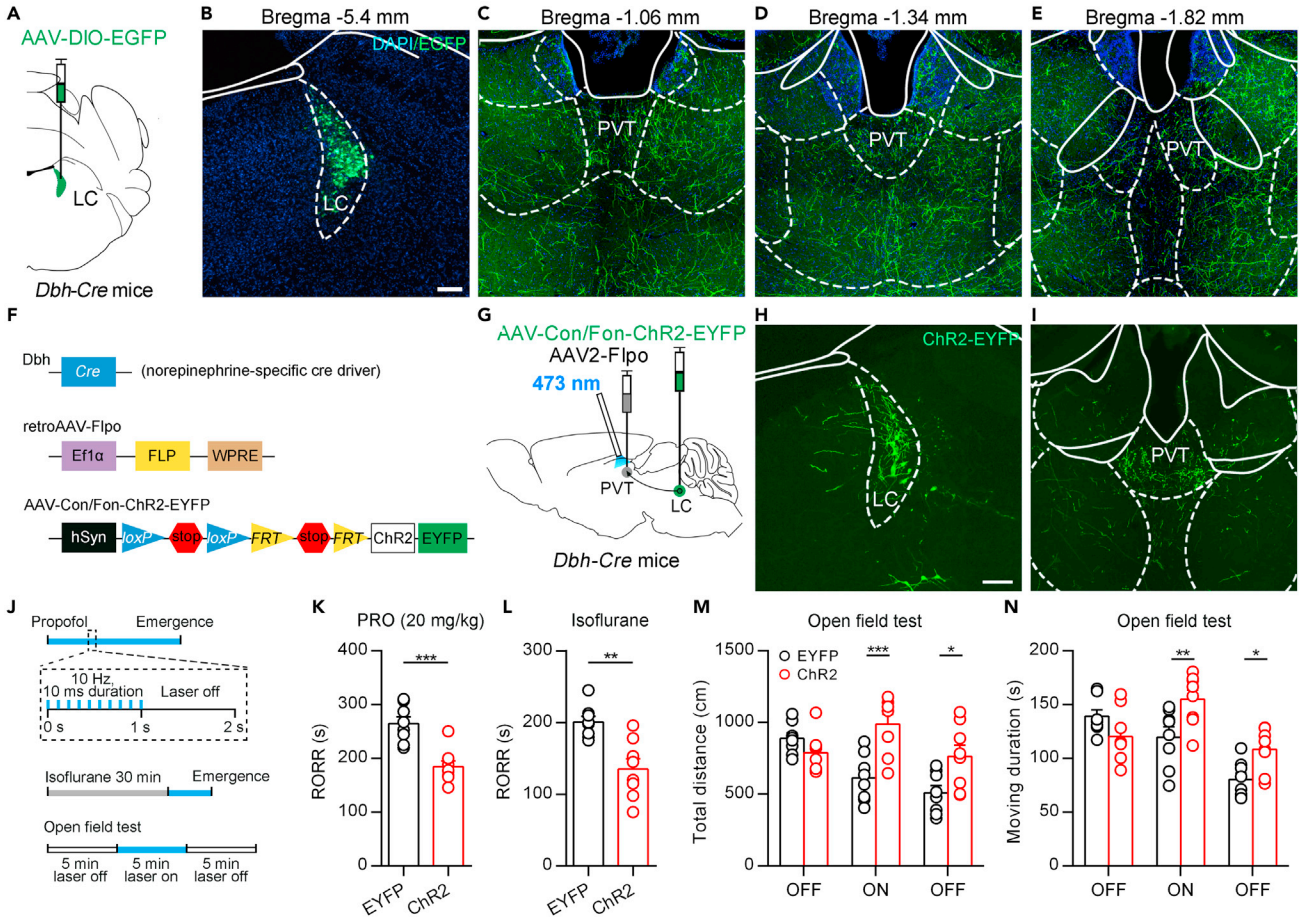


**Figure 1. Optogenetics activation of LC-PVT NE projection**

(A) Schematic showing virus injection to *Dbh-Cre* mice.

(B) Virus infection in LC. Scale bar: 100 μm.

(C–E) The projection fibers in the PVT. Different coronal sections (-1.06 mm, -1.34 mm, -1.82 mm from bregma) for (C), (D) and (E). Same scale bar in (B).

(F) Schematic diagram of the Cre-On/Flpo-On system.

(G) Schematic showing virus injection into the LC and PVT on *Dbh-Cre* mice.

(H and I) Virus infection in the LC (H) and projection fibers in PVT (I). Scale bar: 100 μm.

(J) Schematic diagram of optogenetics activation of LC-PVT NE projection in OFT, propofol-induced anesthesia and isoflurane-induced anesthesia.

(K) RORR of propofol-induced anesthesia in ChR2 mice and control mice. Two-tailed unpaired *t* test, ***$p < 0.001$, n = 8 mice per group.

(L) RORR of isoflurane-induced anesthesia in ChR2 mice and control mice. Two-tailed unpaired *t* test, **$p < 0.01$, n = 8 mice per group.

(M and N) Total distance (M) and moving duration (N) in OFT. two-way ANOVA followed by Bonferroni test, *$p < 0.05$, **$p < 0.01$, ***$p < 0.001$, n = 8 mice per group. Data are represented as mean ± SEM.

spontaneous excitatory postsynaptic currents (sEPSCs) frequency via α1 ARs. In summary, the present study indicates NE modulates wakefulness via α1 adrenoceptors in the PVT. The α1 ARs in the PVT might be a potential central target for understanding wakefulness and general anesthesia mechanisms.

## RESULTS

### Optogenetics activation of LC-PVT projections accelerates emergence from general anesthesia and enhances locomotion activity

The LC NE system is known to have a broad projection throughout the central nervous system (Chandler et al., 2019; Schwarz et al., 2015). To investigate the LC-PVT projections, we injected a Cre-dependent adeno-associated virus (AAV) encoding the enhanced green fluorescent protein (EGFP) (AAV2/8-Ef1α-DIO-EGFP) into the LC of *Dbh-Cre* mice (Figures 1A and 1B). *Dbh-Cre* mice express Cre recombinase under the control of dopamine-b-hydroxylase (*Dbh*) gene promoter, and Dbh is expressed only in catecholamine

cells, including LC NE neurons (Zhao et al., 2017). We found that GFP$^+$ efferent fibers existed throughout the brain, including the PVT (Figures 1C–1E and S1). To specifically label the PVT-projecting LC NE neurons, we injected retrograde AAV2/2-EF1α-Flpo virus into the PVT and AAV2/9-hSyn-CreOn/FlpoOn-ChR2-EYFP virus which encoding the ChR2 fused with the enhanced yellow fluorescent protein (ChR2-EYFP) into the LC of *Dbh-Cre* mice (Figures 1F and 1G). Under this condition, the expression of ChR2-EYFP was dependent on both Cre and Flpo recombinases. Therefore, only LC NE neurons projecting to the PVT expressed ChR2-EYFP (Figure 1H). We found dense EYFP$^+$ fibers in the PVT (Figure 1I). We also examined whether the PVT-projecting LC neurons send collateral projections to other brain areas, such as the hippocampus, somatosensory cortex, and found that these regions had few projection fibers (Figure S2). These results indicate that PVT is a specific downstream projection region of LC NE neurons with few collateral projections to other nuclei.

By using virus labeling and optogenetics, we further specifically activated the LC-PVT NE projection to examine the behavioral emergence from general anesthesia (Figure 1G). We recorded the return of the righting reflex (RORR), which has previously been used as surrogate measures for the resumption of consciousness under anesthesia (Franks, 2008). We found that 10 Hz 473 nm laser pulses significantly decreased the LORR in propofol (intravenously injected, 20 mg/kg)-induced general anesthesia and isoflurane-induced general anesthesia (Figures 1J–1L). On the other side, we also examined locomotion activity in 15 min open field test (OFT), which consisted of 5 min laser off, 5 min 10 Hz laser on, and 5 min laser off (Figure 1J). We found that activation of the LC-PVT NE projection significantly increased total distance and moving duration in the laser on phase (Figures 1M and 1N), indicating more exploratory behaviors and enhanced locomotion ability in ChR2 mice. These results showed that optogenetic activation of the LC-PVT NE projection accelerated emergence from anesthesia and enhanced locomotion.

## Microinjection of NE into the PVT accelerates emergence from general anesthesia and enhances locomotion activity

To further investigate the functional role of NE in the PVT, we implanted the cannula in the PVT and performed the electroencephalography (EEG)/electromyography (EMG) recording on wild-type mice (Figures 2A and 2B). We microinjected NE (240 nL, 2 mM) or artificial cerebrospinal fluid (ACSF) into the PVT and intravenously injected propofol (20 mg/kg) 15 min later. The transitions from anesthesia to wakefulness in the NE group were accelerated compared with the ACSF group (Figure 2C). We also compared the latency to wake (by EEG results) and latency to RORR. We found that there was a corresponding relationship between these two indexes (Figure 2D).

In the EEG/EMG experiment, we left the mice undisturbed and recorded EEG/EMG as well as behavioral RORR. However, researchers often left the anesthetized mice in a slowly rotating cylinder to detect the behavioral RORR accurately (Yip et al., 2013; Zhang et al., 2015). Next, we used the slowly rotating cylinder approach and found that the NE group showed a significantly shortened RORR in propofol-induced anesthesia consistently (Figures 2E–2G). We also examined locomotion activity in the OFT after microinjection of NE into the PVT (Figure 2F). The total distance and moving duration were increased in the NE group (Figures 2H–2J). The center duration and the velocity were not significantly different (Figures 2K and 2L). Taken together, these data further indicated that microinjection of NE into the PVT could accelerate emergence from anesthesia and increase basal locomotion activity.

## NE depolarizes PVT neurons by increasing sEPSCs frequency

We subsequently examined the effects of NE on PVT neurons by whole-cell patch-clamping recordings. We found that the application of 5 μM NE depolarized the membrane potential of PVT neurons (Figures 3A and 3B) and had a nonsignificant increasing tendency of the firing rates ($p = 0.0879$, Figure 3C). Previous studies found that LC drives stress-evoked dopamine release and further induces disinhibition via postsynaptic D2Rs in PVT neurons (Beas et al., 2018). To examine the potential role of D2Rs in NE-induced activation of PVT neurons, we applied 1 μM sulpiride (a D2R antagonist) before 5 μM NE and found that the application of NE still induced similar changes (Figures 3E and 3F). These results indicate that NE could depolarize PVT neurons independently of D2Rs.

We next investigated the mechanisms underlying the NE-mediated depolarizing of PVT neurons. It could be due to the suppression of inhibitory inputs and/or the enhancement of excitatory inputs. To assess these possibilities, we performed whole-cell voltage-clamp recordings of PVT neurons. We first examined the

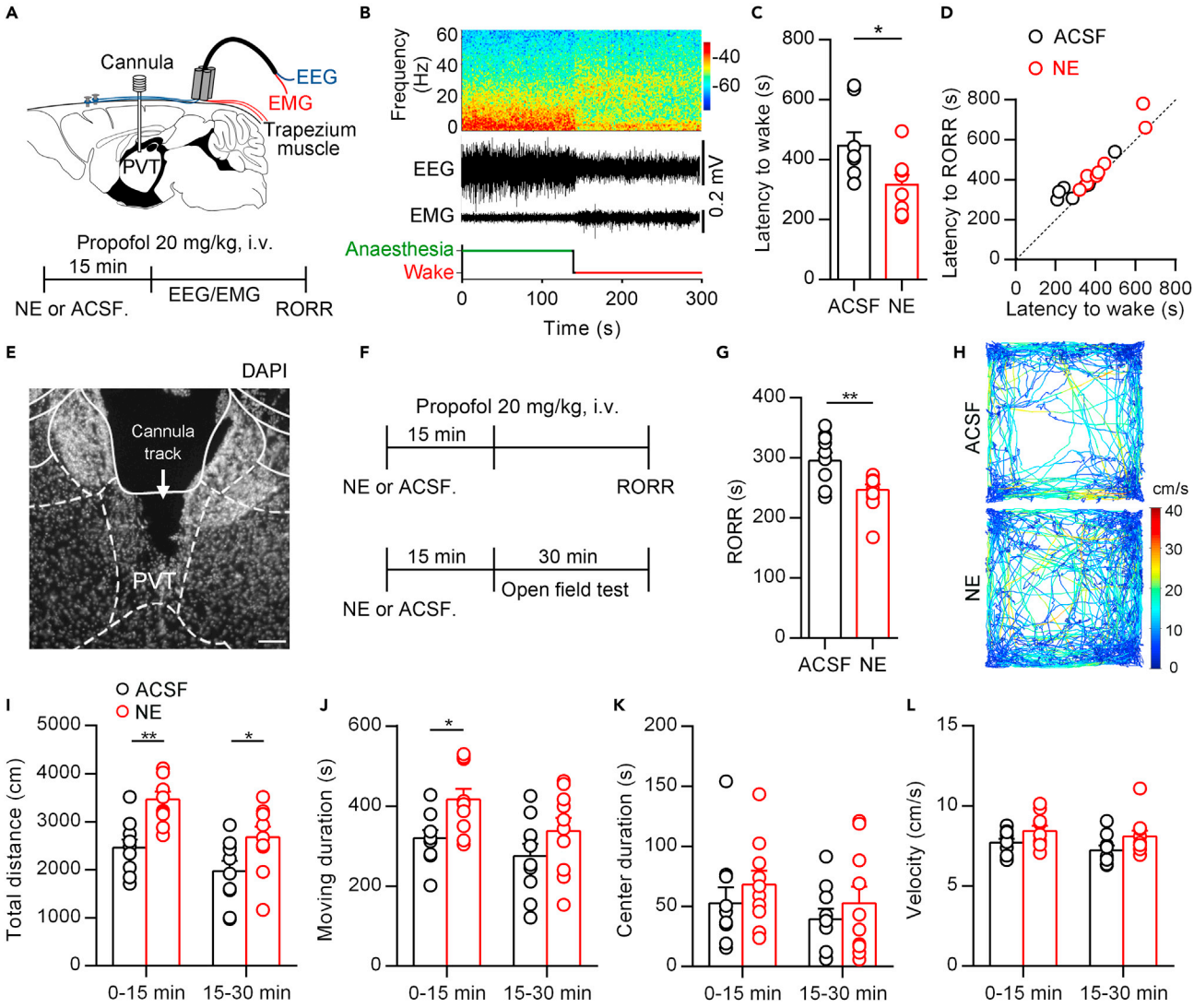


**Figure 2. Microinjection of NE into the PVT accelerates emergence from propofol anesthesia and enhances locomotion**

(A) Schematic of cannula implantation into the PVT and EEG-EMG recordings (top) and timeline for NE (2 mM, 240 nL) or ACSF microinjection in propofol-induced general anesthesia experiment (bottom).

(B) EEG power spectrum and EEG-EMG traces and hypnograms during the transition from propofol-induced anesthesia to wakefulness after NE (2 mM, 240 nL) microinjection into the PVT.

(C) Latency to wakefulness from propofol-induced anesthesia after NE (2 mM, 240 nL) or ACSF microinjection into the PVT. Two-tailed paired t test, *$p < 0.05$, n = 8 mice for each group.

(D) The correlation between latency to wakefulness and RORR from propofol-induced anesthesia after NE (2 mM, 240 nL) or ACSF microinjection into the PVT. The dotted line was the bisector of the first quadrant (Y = X).

(E) Representative DAPI staining images from one mouse implanted with cannula in the PVT. The arrow indicates the cannula track. Scale bar: 100 μm.

(F) Timelines for NE (2 mM, 240 nL) or ACSF microinjection in propofol-induced general anesthesia experiment (top) and open field experiment (bottom).

(G) Propofol-induced RORR in NE (2 mM) or ACSF microinjection experiments. Two-tailed paired *t* test, **$p < 0.01$, n = 10 and 11 mice for each group.

(H) Representative moving tracks from an ACSF microinjected mouse (top) and a NE microinjected mouse (bottom).

(I–L) Total distance (I), move duration (J), center duration (K), and velocity (L) in open field test after microinjection of ACSF or NE into the PVT. two-way ANOVA followed by Bonferroni test, *$p < 0.05$, **$p < 0.01$, n = 10 mice for each group. Data are represented as mean ± SEM.

effect of 5 μM NE on the sEPSCs of PVT neurons (Figures 4A–4E). The application of 5 μM NE increased the frequency of sEPSCs (Figure 4B), but did not affect the amplitude or half-width (Figures 4C and 4D). In addition, 5 μM NE also induced a tonic inward shift of holding currents (Figure 4E). These data indicate that NE enhances the spontaneous excitatory inputs of PVT neurons.

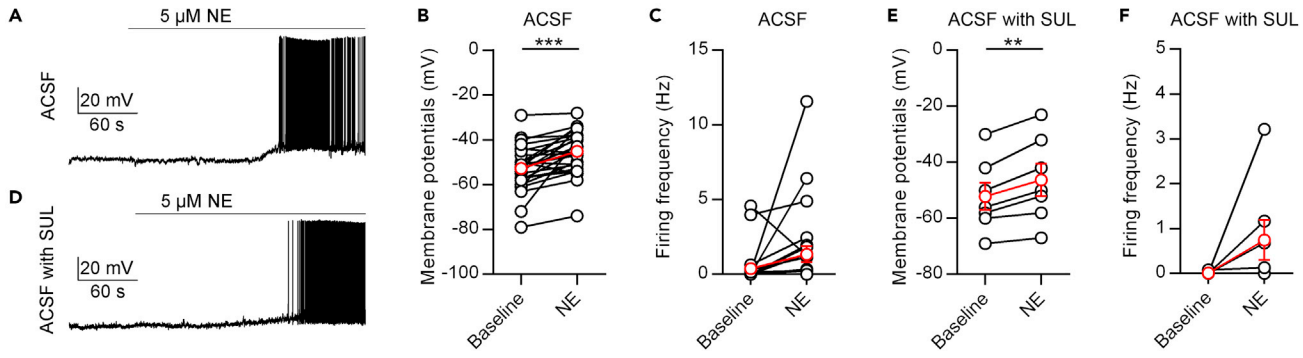


**Figure 3. NE depolarizes PVT neurons in brain slice recording**

(A) A representative neuron shows that NE (5 μM) increases the activity of PVT neurons.

(B and C) Statistical comparison of the membrane potential (B) and firing frequency (C) after application of 5 μM NE. Two-tailed paired *t* test, ***$p < 0.001$, $n = 25$ neurons.

(D) A representative neuron shows that NE (5 μM) increases the activity of PVT neurons in the presence of 5 μM sulpiride (SUL).

(E and F) Statistical comparison of the membrane potential (E) and firing frequency (F) after application of 5 μM NE in the presence of 5 μM SUL. Two-tailed paired *t* test, **$p < 0.01$, $n = 7$ neurons. Data are represented as mean ± SEM.

In contrast to the sEPSCs results, application of 5 μM NE did not significantly affect the frequency, amplitude, or half-width of sIPSCs, nor did it affect the holding currents at 0 mV (Figures 4F–4J), indicating that NE does not enhance the spontaneous inhibitory inputs of PVT neurons.

### NE enhanced the excitatory inputs to PVT neurons mainly via α1 ARs

Next, we examined the receptor mechanisms of NE in the PVT. NE has complex effects depending on the activation of various ARs. Phenylephrine (PHE) is a selective pharmacological agonist of α1 ARs, whereas isoproterenol (ISO) is a nonselective agonist of β ARs (Mei et al., 2013; Zimnik et al., 2013). The application of 5 μM PHE significantly increased the membrane potential and spontaneous firing frequency of PVT neurons (Figures 5A–5C). On the other hand, the application of 5 μM ISO did not affect the membrane potential and spontaneous firing frequency of PVT neurons (Figures 5D–5F). Furthermore, we found that 5 μM PHE increased the sEPSCs frequency but not the amplitude and half-width (Figures 5G–5J), which were consistent with the effects of NE. The holding currents tended to decrease, although not significantly ($p = 0.0782$, Figure 5K). These data indicate that NE enhances the spontaneous excitatory inputs to PVT neurons by acting on α1 ARs.

Previous studies have shown that the changes of sEPSCs frequency are more likely to be caused by presynaptic mechanisms (Du et al., 2018; Zhang et al., 2013). The PVT receives major inputs from the brainstem (LC, PBN, PAG), hypothalamus, prefrontal cortical areas (Kirouac, 2015). Many brain regions upstream of the PVT express *α1 AR* mRNAs in the cytoplasm (from Allen Brain Atlas) and express α1 AR proteins on the membrane (which could not be detected by *in situ* hybridization). We postulated that presynaptic α1 ARs on presynaptic axons might make a major contribution to the increased frequency of sEPSCs. More examinations are needed to dissect the functional upstream regions and subtypes of α1 ARs in modulating wakefulness.

## DISCUSSION

In this study, we systematically investigated the functional role of LC-PVT projections in modulating wakefulness via α1 adrenoceptors in mice. Virus tracing data showed that PVT-projecting LC neurons had few collateral projections. Behavioral tests indicated that optogenetic activation of LC-PVT NE projections or microinjection of NE into the PVT accelerated emergence from anesthesia and enhanced locomotion. Slice recording results confirmed that NE depolarized PVT neurons mainly by increasing sEPSCs frequency via α1 adrenoceptors. Thus, our results demonstrate that NE modulates wakefulness via α1 adrenoceptors in the PVT.

### LC-PVT NE projection modulates emergence and locomotion

The LC NE system broadly projects throughout the central nervous system (Chandler et al., 2019; Schwarz et al., 2015). It is important to highlight that different modalities of stressors activate the LC-NE system, such as restraint, unpredictable shock, and social stress (Godoy et al., 2018; Wood and Valentino, 2017).

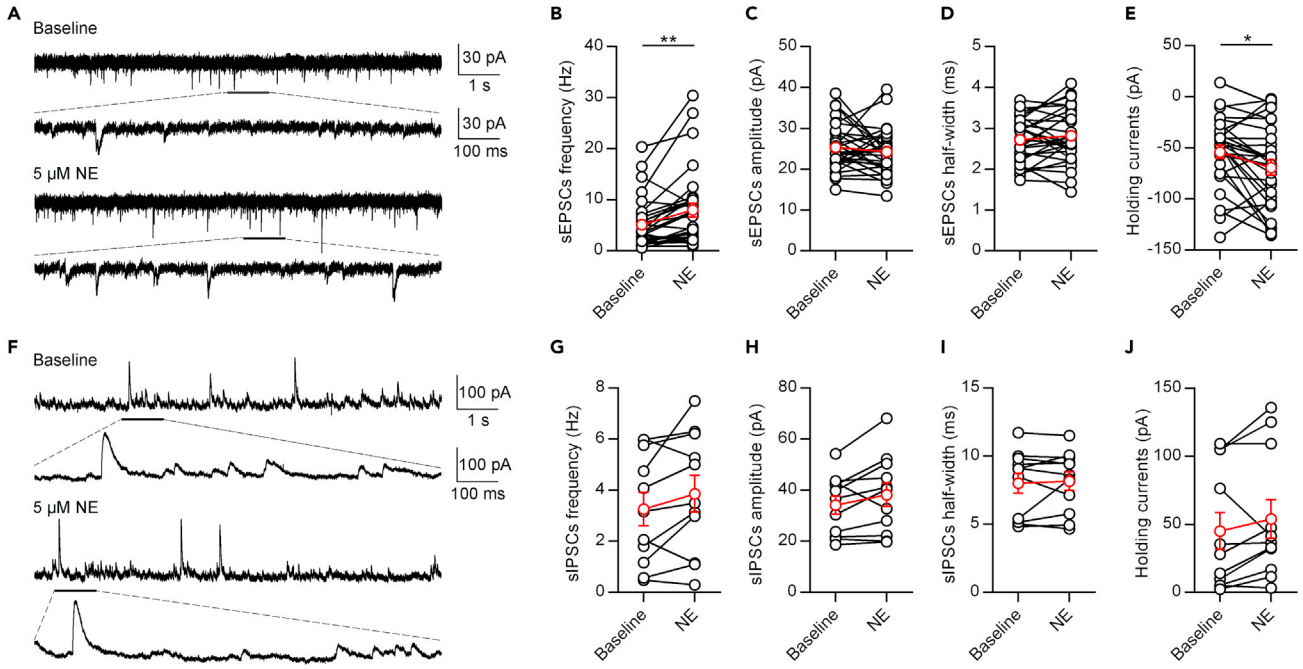


**Figure 4. NE Enhances Excitatory Inputs to PVT Neurons**

(A) A representative neuron shows the effect of NE (5 μM) on spontaneous EPSCs of PVT neurons.

(B–E) Statistical comparison of the frequency (B), amplitude (C), half-width (D) of spontaneous EPSCs and holding currents (E) after application of 5 μM NE. Two-tailed paired *t* test, *p < 0.05, **p < 0.01, n = 30 neurons.

(F) A representative neuron shows the effect of NE (5 μM) on spontaneous IPSCs of PVT neurons.

(G–J) Statistical comparison of the frequency (G), amplitude (H), half-width (I) of spontaneous IPSCs and holding currents (J) after application of 5 μM NE, n = 11 neurons. Data are represented as mean ± SEM.

LC neurons are essential for the high levels of arousal required when responding to salient stimuli and stressors (Scammell et al., 2017; Wood and Valentino, 2017). In the present study, we combined using Cre/*loxP* and Flpo/FRT systems to trace PVT-projecting LC NE neurons and found that PVT is a specific downstream projection region of LC-NE neurons, with few collateral projection patterns. The noradrenergic projection from LC to PVT links these two critical nuclei directly and specifically.

Importantly, we found that optogenetic activation of LC-PVT NE projection or direct microinjection of NE into the PVT accelerated emergence from anesthesia and enhanced locomotion. In a recent study, it was reported that an infusion of NE into the central medial thalamic nucleus accelerates the RORR in propofol-induced anesthesia (Fu et al., 2017). The same study also showed that propofol enhances GABAergic transmission, whereas NE partly reverses these effects. Since the LC NE system has an extensive projection, synergistic effects at the PVT and central medial thalamic nucleus might occur in anesthesia and emergence.

However, it is important to note that the LC lesion has little effect on the amount of wakefulness or sleep during the wake-sleep cycle (Blanco-Centurion et al., 2007; Lu et al., 2006; Saper et al., 2010). Meanwhile, the neuropeptides orexin A and orexin B (also known as hypocretin 1 and hypocretin 2) are crucial in maintaining wakefulness (Li et al., 2014; Sakurai, 2007), and the PVT is regulated by hypocretin$^{+}$ neurons in the lateral hypothalamus (Ren et al., 2018). Furthermore, the histaminergic tuberomammillary nucleus (TMN) is another wake-promoting nucleus (Scammell et al., 2019), and the histaminergic TMN neurons project to the dorsal medial thalamus (Allen brain atlas experiment ID 520336173). These results suggest that the PVT is a critical node in complex neural circuits for controlling wakefulness.

## Role of α1 ARs in increasing sEPSCs frequency to PVT neurons

D2Rs are supposed to be involved in mediating NE's effects in the PVT and other nuclei (Arencibia-Albite et al., 2007; Beas et al., 2018). A previous study found that LC could drive disinhibition of PVT neurons in the restraint stress condition (Beas et al., 2018). They mainly focused on dissecting the changes of miniature

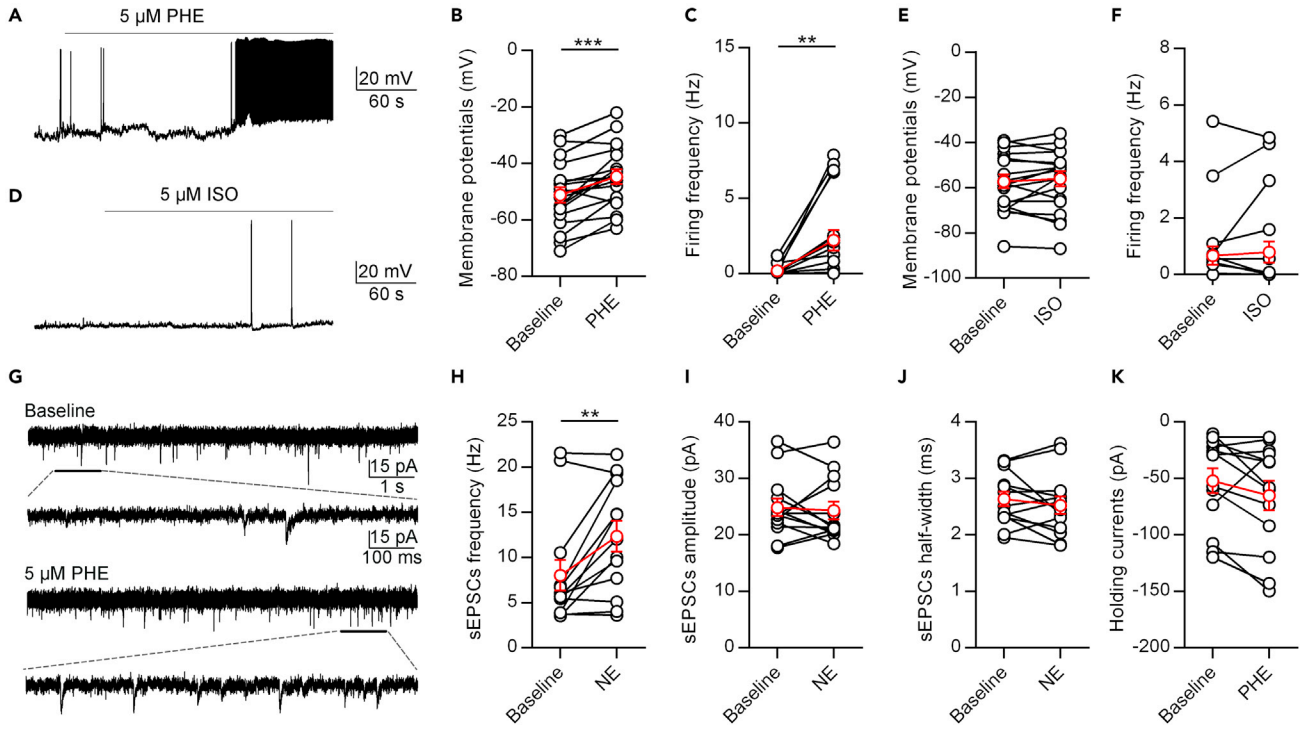


**Figure 5. NE Increases the Activity of PVT Neurons through α1 ARs**

(A) A representative neuron shows that PHE (5 μM) increases the activity of PVT neurons.

(B and C) Statistical Comparison of the membrane potential (B) and firing frequency (C) after application of 5 μM PHE. Two-tailed paired *t* test, $^{**}p < 0.001$, $^{***}p < 0.001$, n = 18 neurons.

(D) A representative neuron shows ISO (5 μM) increases the activity of PVT neurons.

(E and F) Statistical comparison of the membrane potential (E) and firing frequency (F) after application of 5 μM ISO. n = 7 neurons.

(G) A representative neuron shows that the effect of PHE (5 μM) on spontaneous EPSCs of PVT neurons.

(H–K) Statistical comparison of the frequency (H), amplitude (I), half-width (J) of spontaneous EPSCs, and holding currents (K) after application of 5 μM PHE. Two-tailed paired *t* test, $^{**}p < 0.01$, n = 13 neurons. Data are represented as mean ± SEM.

IPSCs in the stress condition by applying D2R agonist quinpirole or antagonist sulpiride. However, the effects of NE on spontaneous EPSCs and spontaneous IPSCs under normal conditions were not clearly examined. In our experiments, we found that NE could depolarize PVT neurons with the presence of D2R antagonist sulpiride. We also found that α1 AR agonist PHE depolarized the membrane potential and increased the firing rate of PVT neurons. Moreover, these effects were achieved mainly by increasing sEPSCs frequency but not by disinhibition mechanisms. These data suggest that co-released dopamine from LC NE neurons acts on postsynaptic PVT neurons, and NE acts on α1 ARs (both presynaptic and postsynaptic). Whether NE and dopamine cooperate in diverse physiological functions needs further examination.

The changes of sEPSCs frequency are more likely to be caused by presynaptic mechanisms (Du et al., 2018; Zhang et al., 2013), and it is strongly associated with presynaptic $Ca^{2+}$ transient (Lee and Kim, 2015). Previous studies have suggested that presynaptic α1 ARs activation leads to increased $Ca^{2+}$ influx and protein kinase C levels, leading to altered synaptic-transmitter release (Kulik et al., 1999; Leenders and Sheng, 2005). Therefore, our results indicate that NE might act on presynaptic α1 ARs and increase synaptic transmission, especially for excitatory synapses. Application of NE or PHE might also activate ARs in postsynaptic neurons. However, it is difficult to separate the pure effect of postsynaptic ARs from presynaptic ARs. Whether postsynaptic ARs participate in the effects of NE on PVT neurons requires further genetics ablation study.

In summary, we have identified the critical role of NE in modulating the activity of PVT neurons in emergence from anesthesia and locomotion. Moreover, we elucidated the electrophysiological mechanisms

underlying the effects of NE on PVT neurons. Finally, we suggest that the α1 ARs in the PVT is a potential central target for increasing understanding of general anesthesia mechanisms and developing new general anesthetics.

### Limitations of the study

This study has not examined the suppression of LC-PVT NE projections on emergence from anesthesia and locomotion. Furthermore, the functional role of the postsynaptic α1 ARs on PVT neurons is unknown. Future studies will be required to fully dissect the contribution of presynaptic and postsynaptic α1 ARs in the PVT in modulating wakefulness.

## STAR★METHODS

Detailed methods are provided in the online version of this paper and include the following:

- KEY RESOURCES TABLE
- RESOURCE AVAILABILITY
  - Lead contact
  - Materials availability
  - Data and code availability statement
- EXPERIMENTAL MODEL AND SUBJECT DETAILS
- METHOD DETAILS
  - Stereotaxic surgery for injection into the LC and PVT
  - Optic fiber implantation into the PVT and optogenetics manipulation
  - Cannula implantation into the PVT and NE microinjection
  - Electroencephalogram (EEG) and electromyography (EMG)
  - Propofol-induced general anesthesia
  - Isoflurane-induced general anesthesia
  - Open field test
  - Immunohistochemistry
  - Brain slice electrophysiology
  - Data acquisition and analysis
- QUANTIFICATION AND STATISTICAL ANALYSIS

## SUPPLEMENTAL INFORMATION

Supplemental information can be found online at https://doi.org/10.1016/j.isci.2021.103015.

## ACKNOWLEDGMENTS

We thank Dr. Cheng Zhan (the National Institute of Biological Sciences, Beijing, China) for the gift of *Dbh-Cre* transgenic mice. We thank Dr. Xing-Jun Liu (Shantou University Medical College, Shantou, China) and Dr. Wen-Li Mi (Fudan University, Shanghai, China) for critical reading of the manuscript. We thank Enago (http://www.enago.com/) for the English language review. This work was supported by the National Natural Science Foundation of China (No. 31900717, to D.M.), the Shanghai Sailing Program from Shanghai Association for Science and Technology (19YF1438700, to D.M.), the Youth Talent Support Program from China Association for Science and Technology (2019QNRC001, to D.M.), Youth talent support program from Shanghai Jiao Tong University School of Medicine (19XJ11010, to D.M.).

## AUTHOR CONTRIBUTIONS

J.-B.L., L.-N.H., and D.M. designed research; Y.W., L.X., M.-Z.L., F.F., and D.-J.X. performed virus injection and behavioral tests; L.X. and R.Z. performed patch-clamping recordings. X.-X.H. and L.Z. performed EEG/EMG recordings. Y.W. performed the immunohistochemical experiments and analyzed data. Y.W. and D.M. wrote the paper.

## DECLARATION OF INTERESTS

The manuscript has not been published previously and is not under consideration for publication elsewhere. All authors declare that there are no competing financial interests in this study.

Received: March 1, 2021
Revised: July 10, 2021
Accepted: August 18, 2021
Published: September 24, 2021

## REFERENCES

Adamantidis, A.R., Gutierrez Herrera, C., and Gent, T.C. (2019). Oscillating circuitries in the sleeping brain. Nat. Rev. Neurosci. *20*, 746–762. https://doi.org/10.1038/s41583-019-0223-4.

Arencibia-Albite, F., Paladini, C., Williams, J.T., and Jiménez-Rivera, C.A. (2007). Noradrenergic modulation of the hyperpolarization-activated cation current (Ih) in dopamine neurons of the ventral tegmental area. Neuroscience *149*, 303–314. https://doi.org/10.1016/j.neuroscience.2007.08.009.

Barresi, M., Grasso, C., Licata, F., and Li Volsi, G. (2014). Noradrenergic modulation of neuronal responses to n-methyl-d-aspartate in the vestibular nuclei: an electrophysiological and immunohistochemical study. Neuroscience *265*, 172–183. https://doi.org/10.1016/j.neuroscience.2014.01.054.

Beas, B.S., Wright, B.J., Skirzewski, M., Leng, Y., Hyun, J.H., Koita, O., Ringelberg, N., Kwon, H.B., Buonanno, A., and Penzo, M.A. (2018). The locus coeruleus drives disinhibition in the midline thalamus via a dopaminergic mechanism. Nat. Neurosci. *21*, 963–973. https://doi.org/10.1038/s41593-018-0167-4.

Blanco-Centurion, C., Gerashchenko, D., and Shiromani, P.J. (2007). Effects of saporin-induced lesions of three arousal populations on daily levels of sleep and wake. J. Neurosci. *27*, 14041–14048. https://doi.org/10.1523/JNEUROSCI.3217-07.2007.

Breton-Provencher, V., and Sur, M. (2019). Active control of arousal by a locus coeruleus GABAergic circuit. Nat. Neurosci. *22*, 218–228. https://doi.org/10.1038/s41593-018-0305-z.

Carter, M.E., Yizhar, O., Chikahisa, S., Nguyen, H., Adamantidis, A., Nishino, S., Deisseroth, K., and De Lecea, L. (2010). Tuning arousal with optogenetic modulation of locus coeruleus neurons. Nat. Neurosci. *13*, 1526–1535. https://doi.org/10.1038/nn.2682.

Chandler, D.J., Jensen, P., McCall, J.G., Pickering, A.E., Schwarz, L.A., and Totah, N.K. (2019). Redefining noradrenergic neuromodulation of behavior: impacts of a modular locus coeruleus architecture. J. Neurosci. *39*, 8239–8249. https://doi.org/10.1523/JNEUROSCI.1164-19.2019.

Church, T.W., Brown, J.T., and Marrion, N.V. (2019). β3-Adrenergic receptor-dependent modulation of the medium afterhyperpolarization in rat hippocampal CA1 pyramidal neurons. J. Neurophysiol. *121*, 773–784. https://doi.org/10.1152/jn.00334.2018.

Du, W.-J., Zhang, R.-W., Li, J., Zhang, B.-B., Peng, X.-L., Cao, S., Yuan, J., Yuan, C.-D., Yu, T., and Du, J.-L. (2018). The locus coeruleus modulates intravenous general anesthesia of zebrafish via a cooperative mechanism. Cell Rep. *24*, 3146–3155.e3. https://doi.org/10.1016/j.celrep.2018.08.046.

Franks, N.P. (2008). General anaesthesia: from molecular targets to neuronal pathways of sleep and arousal. Nat. Rev. Neurosci. *9*, 370–386. https://doi.org/10.1038/nrn2372.

Fu, B., Yu, T., Yuan, J., Gong, X., and Zhang, M. (2017). Noradrenergic transmission in the central medial thalamic nucleus modulates the electroencephalographic activity and emergence from propofol anesthesia in rats. J. Neurochem. *140*, 862–873. https://doi.org/10.1111/jnc.13939.

Godoy, L.D., Rossignoli, M.T., Delfino-Pereira, P., Garcia-Cairasco, N., and Umeoka, E.H.de L. (2018). A comprehensive overview on stress neurobiology: basic concepts and clinical implications. Front. Behav. Neurosci. *12*, 1–23. https://doi.org/10.3389/fnbeh.2018.00127.

Grzelka, K., Kurowski, P., Gawlak, M., and Szulczyk, P. (2017). Noradrenaline modulates the membrane potential and holding current of medial prefrontal cortex pyramidal neurons via β1-adrenergic receptors and HCN channels. Front. Cell. Neurosci. *11*, 1–22. https://doi.org/10.3389/fncel.2017.00341.

Gu, Q. (2002). Neuromodulatory transmitter systems in the cortex and their role in cortical plasticity. Neuroscience *111*, 815–835. https://doi.org/10.1016/S0306-4522(02)00026-X.

Hayat, H., Regev, N., Matosevich, N., Sales, A., Paredes-Rodriguez, E., Krom, A.J., Bergman, L., Li, Y., Lavigne, M., Kremer, E.J., et al. (2020). Locus coeruleus norepinephrine activity mediates sensory-evoked awakenings from sleep. Sci. Adv. *6*, eaaz4232. https://doi.org/10.1126/sciadv.aaz4232.

Kirouac, G.J. (2015). Placing the paraventricular nucleus of the thalamus within the brain circuits that control behavior. Neurosci. Biobehav. Rev. *56*, 315–329. https://doi.org/10.1016/j.neubiorev.2015.08.005.

Kulik, A., Haentzsch, A., Lückermann, M., Reichelt, W., and Ballanyi, K. (1999). Neuron-glia signaling via α1 adrenoceptor-mediated $Ca^{2+}$ release in Bergmann glial cells in situ. J. Neurosci. *19*, 8401–8408. https://doi.org/10.1523/JNEUROSCI.19-19-08401.1999.

Lee, S.Y., and Kim, J.H. (2015). Mechanisms underlying presynaptic $Ca^{2+}$ transient and vesicular glutamate release at a CNS nerve terminal during in vitro ischaemia. J. Physiol. *593*, 2793–2806. https://doi.org/10.1113/JP270060.

Leenders, A.G.M., and Sheng, Z.H. (2005). Modulation of neurotransmitter release by the second messenger-activated protein kinases: implications for presynaptic plasticity. Pharmacol. Ther. *105*, 69–84. https://doi.org/10.1016/j.pharmthera.2004.10.012.

Li, J., Hu, Z., and de Lecea, L. (2014). The hypocretins/orexins: integrators of multiple physiological functions. Br. J. Pharmacol. *171*, 332–350. https://doi.org/10.1111/bph.12415.

Lu, J., Sherman, D., Devor, M., and Saper, C.B. (2006). A putative flip-flop switch for control of REM sleep. Nature *441*, 589–594. https://doi.org/10.1038/nature04767.

Mei, Y., Yin, N., Jin, X., He, J., and Yin, Z. (2013). The regulatory role of the adrenergic agonists phenylephrine and isoproterenol on fetal hemoglobin expression and erythroid differentiation. Endocrinology *154*, 4640–4649. https://doi.org/10.1210/en.2013-1535.

Pieribone, V.A., Nicholas, A.P., Dagerlind, A., and Hokfelt, T. (1994). Distribution of α1 adrenoceptors in rat brain revealed by in situ hybridization experiments utilizing subtype-specific probes. J. Neurosci. *14*, 4252–4268. https://doi.org/10.1523/jneurosci.14-07-04252.1994.

Rainbow, T.C., Parsons, B., and Wolfe, B.B. (1984). Quantitative autoradiography of beta 1- and beta 2-adrenergic receptors in rat brain. Proc. Natl. Acad. Sci. U S A *81*, 1585–1589. https://doi.org/10.1073/pnas.81.5.1585.

Ren, S., Wang, Y., Yue, F., Cheng, X., Dang, R., Qiao, Q., Sun, X., Li, X., Jiang, Q., Yao, J., et al. (2018). The paraventricular thalamus is a critical thalamic area for wakefulness. Science *362*, 429–434. https://doi.org/10.1126/science.aat2512.

Rosin, D.L., Talley, E.M., Lee, A., Stornetta, R.L., Gaylinn, B.D., Guyenet, P.G., and Lynch, K.R. (1996). Distribution of α2C-adrenergic receptor-like immunoreactivity in the rat central nervous system. J. Comp. Neurol. *372*, 135–165. https://doi.org/10.1002/(sici)1096-9861(19960812)372:1<135::aid-cne9>3.0.co;2-4.

Sakurai, T. (2007). The neural circuit of orexin (hypocretin): maintaining sleep and wakefulness. Nat. Rev. Neurosci. *8*, 171–181. https://doi.org/10.1038/nrn2092.

Saper, C.B., Fuller, P.M., Pedersen, N.P., Lu, J., and Scammell, T.E. (2010). Sleep state switching. Neuron *68*, 1023–1042. https://doi.org/10.1016/j.neuron.2010.11.032.

Sara, S.J. (2009). The locus coeruleus and noradrenergic modulation of cognition. Nat. Rev. Neurosci. *10*, 211–223. https://doi.org/10.1038/nrn2573.

Scammell, T.E., Arrigoni, E., and Lipton, J.O. (2017). Neural circuitry of wakefulness and sleep. Neuron *93*, 747–765. https://doi.org/10.1016/j.neuron.2017.01.014.

Scammell, T.E., Jackson, A.C., Franks, N.P., Wisden, W., and Dauvilliers, Y. (2019). Histamine:

neural circuits and new medications. Sleep *42*, 1–8. https://doi.org/10.1093/sleep/zsy183.

Schwarz, L.A., Miyamichi, K., Gao, X.J., Beier, K.T., Weissbourd, B., Deloach, K.E., Ren, J., Ibanes, S., Malenka, R.C., Kremer, E.J., and Luo, L. (2015). Viral-genetic tracing of the input–output organization of a central noradrenaline circuit. Nature *524*, 88–92. https://doi.org/10.1038/nature14600.

Szabadi, E. (2013). Functional neuroanatomy of the central noradrenergic system. J. Psychopharmacol. *27*, 659–693. https://doi.org/10.1177/0269881113490326.

Vazey, E.M., and Aston-Jones, G. (2014). Designer receptor manipulations reveal a role of the locus coeruleus noradrenergic system in isoflurane general anesthesia. Proc. Natl. Acad. Sci. U S A *111*, 3859–3864. https://doi.org/10.1073/pnas.1310025111.

Vertes, R.P., Linley, S.B., and Hoover, W.B. (2015). Limbic circuitry of the midline thalamus. Neurosci. Biobehav. Rev. *54*, 89–107. https://doi.org/10.1016/j.neubiorev.2015.01.014.

Weber, F., and Dan, Y. (2016). Circuit-based interrogation of sleep control. Nature *538*, 51–59. https://doi.org/10.1038/nature19773.

Wood, S.K., and Valentino, R.J. (2017). The brain norepinephrine system, stress and cardiovascular vulnerability. Neurosci. Biobehav. Rev. *74*, 393–400. https://doi.org/10.1016/j.neubiorev.2016.04.018.

Yip, G.M.S., Chen, Z.-W., Edge, C.J., Smith, E.H., Dickinson, R., Hohenester, E., Townsend, R.R., Fuchs, K., Sieghart, W., Evers, A.S., and Franks, N.P. (2013). A propofol binding site on mammalian GABAA receptors identified by photolabeling. Nat. Chem. Biol. *9*, 715–720. https://doi.org/10.1038/nchembio.1340.

Zhang, Z., Cordeiro Matos, S., Jego, S., Adamantidis, A., and Séguéla, P. (2013). Norepinephrine drives persistent activity in prefrontal cortex via synergistic α1 and α2 adrenoceptors. PLoS One *8*, e66122. https://doi.org/10.1371/journal.pone.0066122.

Zhang, Z., Ferretti, V., Güntan, I., Moro, A., Steinberg, E.A., Ye, Z., Zecharia, A.Y., Yu, X., Vyssotski, A.L., Brickley, S.G., et al. (2015). Neuronal ensembles sufficient for recovery sleep and the sedative actions of α 2 adrenergic agonists. Nat. Neurosci. *18*, 553–561. https://doi.org/10.1038/nn.3957.

Zhao, Z., Wang, L., Gao, W., Hu, F., Zhang, J., Ren, Y., Lin, R., Feng, Q., Cheng, M., Ju, D., et al. (2017). A central catecholaminergic circuit controls blood glucose levels during stress. Neuron *95*, 138–152.e5. https://doi.org/10.1016/j.neuron.2017.05.031.

Zimnik, N.C., Treadway, T., Smith, R.S., and Araneda, R.C. (2013). α1A-Adrenergic regulation of inhibition in the olfactory bulb. J. Physiol. *591*, 1631–1643. https://doi.org/10.1113/jphysiol.2012.248591.

## STAR★METHODS

### KEY RESOURCES TABLE

| REAGENT or RESOURCE | SOURCE | IDENTIFIER |
|---|---|---|
| Bacterial and virus strains | | |
| AAV2/8-EF1α-DIO-EGFP | Shanghai Taitool Co., Ltd | Cat# S0270-8 |
| AAV2/9-hSyn-Con/Fon-ChR2-EYFP | BrainVTA Co., Ltd | Cat# PT-0065 |
| AAV2/9-hSyn-Con/Fon-EYFP | Shanghai Biogene Co., Ltd | Cat# B066-9 |
| retroAAV2/2-EF1α-Flpo | BrainVTA Co.,Ltd | Cat# PT-0144 |
| Chemicals, peptides, and recombinant proteins | | |
| Sulpiride | Macklin | Cat# 23672-07-3 |
| Propofol | Beijing Fresenius Kabi Co., Ltd | N/A |
| Norepinephrine bitartrate injection | Shanghai Harvest Pharmaceutical Co., Ltd | N/A |
| Phenylephrine hydrochloride injection | Shanghai Harvest Pharmaceutical Co., Ltd | N/A |
| Isoprenaline hydrochloride injection | Shanghai Harvest Pharmaceutical Co., Ltd | N/A |
| Experimental models: organisms/strains | | |
| Mouse:C57BL/6J | Shanghai SLAC Laboratory Animal Co.,Ltd | N/A |
| Mouse: Dbh-Cre | MMRRC | MMRRC_036734-UCD |
| Software and algorithms | | |
| Fiji | Fiji | https://imagej.net/software/fiji/ |
| GraphPad Prism 6.0 | GraphPad Software | https://graphpad-prism.software.informer.com/6.0/ |
| Clampfit 10.6 | Molecular Devices | https://www.moleculardevices.com.cn/products/axon-patch-clamp-system/acquisition-and-analysis-software/pclamp-software-suite |
| Videotrack | ViewPoint Behavior Technology | http://www.viewpoint.fr/zh_CN/p/software/videotrack |
| AniLab software | AniLab Software & Instruments Co., Ltd. | http://www.anilab.cn/soft/anilab.asp |
| MATLAB 2013b | MathWorks | https://www.mathworks.com/downloads |

### RESOURCE AVAILABILITY

#### Lead contact

Further information and requests for resources and reagents should be directed to and will be fulfilled by the lead contact, Di Mu (damonmu@163.com or 018501md@shgh.cn).

#### Materials availability

This study did not generate new unique reagents.

#### Data and code availability statement

All relevant datasets and analysis are included in this article and in the supplementary material, or are available from the lead contact upon reasonable request.

All original code is available from the Lead Contact upon reasonable request.

Any additional information required to reanalyze the data reported in this work paper is available from the Lead Contact upon request.

## EXPERIMENTAL MODEL AND SUBJECT DETAILS

Postnatal days (P) 40 male wild-type *C57BL/6J* mice (purchased from SLAC laboratory, China) and P40 male *Dbh-Cre* mice (MMRRC_036734-UCD, gifted by Dr. Cheng Zhan, National Institute of Biological Sciences, China) were used for experiments. All mice were raised on a 12-hr light/dark cycle (lights on at 7:00 am) with *ad libitum* food and water. All behavioral tests were carried out during the light phase. All animal experiment procedures were approved by the Animal Care and Use Committee of the Animal Care and Use Committee of Shanghai General Hospital.

## METHOD DETAILS

### Stereotaxic surgery for injection into the LC and PVT

Mice were anesthetized by vaporized sevoflurane (induction, 3%; maintenance, 1.5%) and head-fixed in a mouse stereotaxic apparatus (RWD Life Science Co.) with a heating pad to maintain the body temperature. An incision was made along the midline and the surface of the skull was exposed. To detect LC NE system's projection, *Dbh-Cre* mice were injected 200 nl AAV2/8-EF1α-DIO-EGFP (AAV2/8, titer: 4 x $10^{12}$ vector genomes (v.g.)/ml, Taitool, China) into the LC (antero-posterior (AP) -5.4 mm, medio-lateral (ML) 0.85 mm, dorsal-ventral (DV) -3.75 mm). To detect the LC-PVT projection, *Dbh-Cre* mice were injected 200 nl AAV2/9-hSyn-CreOn/FlpoOn-ChR2-EYFP (AAV2/9, titer: 4 x $10^{12}$ v.g./ml, BrainVTA, China) into the LC (AP -5.4 mm, ML 0.85 mm, DV -3.75 mm) and 200 nl retroAAV2/2-EF1α-Flpo (AAV2/2, titer: 4 x $10^{12}$ v.g./ml, BrainVTA) into the PVT (AP -1.34 mm, ML 0 mm, DV -2.9 mm). To optogenetics activation of the LC-PVT NE projection, *Dbh-Cre* mice were injected 200 nl AAV2/9-hSyn-Con/Fon-ChR2-EYFP (AAV2/9, titer: 4 x $10^{12}$ v.g./ml, BrainVTA, China) or AAV2/9-hSyn-Con/Fon-EYFP (AAV2/9, titer: 4 x $10^{12}$ v.g./ml, Biogene, China) into the LC (AP -5.4 mm, ML 0.85 mm, DV -3.75 mm) and 200 nl retroAAV2/2-EF1α-Flpo (AAV2/2, titer: 4 x $10^{12}$ v.g./ml, BrainVTA) into the PVT (AP -1.34 mm, ML 0 mm, DV -2.9 mm). The virus was delivered with a glass pipette (tip diameter 10-20 μm) at a rate of 50 nl/min using Picospritzer III (Parker, USA), controlled by Master-8 (A.M.P.I.). After the injection, the glass pipettes were left in place for 10 min withdrawal. All experiments were performed 3-4 weeks after virus injection.

### Optic fiber implantation into the PVT and optogenetics manipulation

After anaesthetization and skull explosion, a 200 μm diameter optic fiber was implanted over the PVT. The optic fiber was attached to the skull with dental cement. After optic fiber implantation, mice recovered for at least 4 weeks before behavioral tests. For activating the LC-PVT NE projection, a 473 nm blue laser (10 Hz, 10 ms pulse duration, 5 mW, Crystalaser CL-473-050) was delivered for 1 second every 2 seconds (Figure 1J).

### Cannula implantation into the PVT and NE microinjection

After anaesthetization and skull explosion, a guide cannula (O.D. 0.41 mm x I.D. 0.25 mm, length: 6.0 mm, RWD Life Science, China) was implanted into the PVT (AP -1.34 mm, ML 0 mm, DV -2.9 mm) of wild-type mice. The guide cannula was attached to the skull with dental cement. After cannula implantation, mice recovered for at least 2 weeks before intracranial injection. 2 mM NE was freshly dissolved in ACSF before injection. NE and ACSF were infused at a rate of 240 nl/min for 1 min (total infused volume: 240 nl), and the injection needle was stayed for an additional 2 min to allow drug diffusion. Experimental mice were randomly divided into two groups: the NE group and the ACSF group.

### Electroencephalogram (EEG) and electromyography (EMG)

After cannula implantation into the PVT, four copper screws were installed at the 1 mm anterior to bregma and 1 mm anterior to the lambda with 1.5 mm lateral on both sides of the skull without penetrating the underlying dura. Fifteen minutes after NE or ACSF injection, the mice were anaesthetized by intravenous injection of propofol (20 mg/kg), 10 mg/ml propofol was injected in a volume of 50 μl/25 g body weight and followed by EEG and EMG recording. The EEG-EMG signals were band-pass filtered (EEG: 0.3-30 Hz, EMG: 10-100 Hz). By using the Spike2 analysis software, the polygraphic recording signal was automatically analyzed in 4 seconds epochs based on spectral signatures of EEG-EMG waveforms. A high EMG together with an intermediate θ (6–10 Hz) to δ (1–4 Hz) ratio was scored as waking state (WAKE), and a low EMG together with high δ and a low θ to δ ratio was scored as anesthesia state. A time-frequency diagram of LFP was performed using a short-time Fourier transform in nonoverlapping 1024 ms Hanning window with a step size of 1 second (NFFT = 2048). The latency to wake or righting reflex was calculated from

the time point when mice were anaesthetized by propofol PVT to the state transitions (onset of cortical activation or behavioral arousal).

### Propofol-induced general anesthesia

Fifteen minutes after NE or ACSF injection, the mice were anaesthetized by intravenous injection of propofol (20 mg/kg). After propofol injection, emergence time from propofol anesthesia was calculated by measuring the time taken for the return of the righting reflex (RORR). Throughout the experiment, the animal was placed inside a continuously rotating (at 3 rpm) chamber, and loss of righting reflex defined as the point when the animal rolled onto its side and all four paws left the surface of the rotating tube and did not attempt to the right itself.

### Isoflurane-induced general anesthesia

Mice were initially anaesthetized using 2% isoflurane in 100% oxygen (2 L/min), then 1.5% isoflurane was continuously delivered after the induction by an isoflurane vaporizer (Howard apparatus). For the emergence from the general anesthesia experiment, mice were anaesthetized for 30 minutes before the discontinuation of isoflurane and RORR was calculated.

### Open field test

Fifteen minutes after injection of NE or ACSF, mice were placed in polystyrene enclosures (40 x 40 x 40 cm) for 30 minutes to test their locomotor activity. Mice were placed in the center of the box and were videotaped individually. The center area was defined as centric 20 x 20 cm. The track was analyzed by Viewpoint software and AniLab software. Total distance traveled, move duration, velocity, and the time spent in the center area were analyzed.

### Immunohistochemistry

Mice were intraperitoneally anaesthetized with pentobarbital sodium (100 mg/kg) and perfused with 0.9% saline through the heart, followed by 4% paraformaldehyde. Brains were first fixed in 4% paraformaldehyde overnight at 4°C and then dehydrated in 30% sucrose at 4°C for 2-3 days. Free-floating brain sections were sectioned at 40 μm thickness with the Cryostat (Leica CM 1860, Germany). Then the sections were incubated with DAPI (1:5000, Beyotime C1002, China) for 10 min. The sections were cover-slipped with fluorescent mounting medium and stored at 4°C before imaging.

### Brain slice electrophysiology

Mice were anaesthetized with isoflurane and perfused transcardially with an ice-cold cutting solution containing (in mM): sucrose 213, KCl 2.5, $NaH_2PO_4$ 1.25, $MgSO_4$ 10, $CaCl_2$ 0.5, $NaHCO_3$ 26, glucose 11 (300-305 mOsm). Then the brain was rapidly dissected, and coronal slices (280 μm) were sectioned, using a vibratome (V1200S, Leica) at a slicing speed of 0.12 mm/s and a blade vibration amplitude of 0.8 mm. Slices were transferred into holding chamber and incubated in 34°C artificial cerebrospinal fluid (ACSF) containing (in mM): NaCl 126, KCl 2.5, $NaH_2PO_4$ 1.25, $MgCl_2$ 2, $CaCl_2$ 2, $NaHCO_3$ 26, glucose 10 (300-305 mOsm). After 30 min recovery, slices were kept at room temperature. Both cutting solution and ACSF were continuously bubbled with 95% $O_2$/5% $CO_2$. All experiments were performed at near-physiological temperatures (30-32°C) using an in-line heater (Warner Instruments) while perfusing the recording chamber with ACSF at 3 ml/min using a pump (HL-1, Shanghai Huxi). Whole-cell patch-clamp recordings were made from the target neurons under IR-DIC visualization and a CCD camera (Retiga ELECTRO, QIMAGING) using a fluorescent Olympus BX51WI microscope. Recording pipettes (2-5 MΩ; Borosilicate Glass BF 150-86-10; Sutter Instrument) were prepared by a micropipette puller (P97; Sutter Instrument) and backfilled with potassium-based internal solution containing (in mM) K-gluconate 130, $MgCl_2$ 1, $CaCl_2$ 1, KCl 1, HEPES 10, EGTA 11, Mg-ATP 2, Na-GTP 0.3 (pH 7.3, 290 mOsm) or cesium-based internal solution contained (in mM) $CsMeSO_3$ 130, $MgCl_2$ 1, $CaCl_2$ 1, HEPES 10, QX-314 2, EGTA 11, Mg-ATP 2, Na-GTP 0.3 (pH 7.3, 295 mOsm). Biocytin (0.2%) was included in the internal solution.

In dissecting the effects of NE or agonists of ARs on membrane potential and firing rates of PVT neurons, neurons in the PVT were recorded in current-clamp I = 0 modem (potassium-based internal solution). After stable recording spontaneous firing for 3 minutes, 5 μM NE, 5 μM phenylephrine, or 5 μM isoproterenol was bath applied for 5 to 10 minutes.

In dissecting the effects of NE or phenylephrine on spontaneous EPSCs or IPSCs of PVT neurons, neurons in the PVT were recorded in voltage-clamp mode (cesium-based internal solution). After stable recording spontaneous EPSCs or IPSCs for 3 minutes, 5 μM NE, or 5 μM phenylephrine was bath applied for 5 to 10 minutes.

To examine the potential role of dopamine receptor 2 (D2R) in NE-induced activation of PVT neurons, neurons in the PVT were recorded in current-clamp I = 0 modem (potassium-based internal solution). After stable recording spontaneous firing for 3 minutes, 1 μM sulpiride (D2R antagonist) was bath applied before 5 μM NE.

Sulpiride were purchased from Macklin (China). Propofol injection was purchased from Beijing Fresenius Kabi Co., Ltd (China). Norepinephrine bitartrate injection, phenylephrine hydrochloride injection, and isoprenaline hydrochloride injection were purchased from Shanghai Harvest Pharmaceutical Co., Ltd (China). All other chemicals were obtained from Sigma-Aldrich.

### Data acquisition and analysis

Voltage-clamp and current-clamp recordings were carried out using a computer-controlled amplifier (MultiClamp 700B; Molecular Devices, USA). During recordings, traces were low-pass filtered at 4 kHz and digitized at 10 kHz (DigiData 1550B1; Molecular Devices). Data were acquired by Clampex 10.6 and filtered using a low-pass-Gaussian algorithm (-3 dB cutoff frequency = 1,000 Hz) in Clampfit 10.6 (Molecular Devices). Extremely small, low signal-to-noise ratio and unreliable responses were regarded as no response. sEPSCs or sIPSCs were analyzed by event detection using well-defined templates in Clampfit 10.6.

## QUANTIFICATION AND STATISTICAL ANALYSIS

All experiments were conducted in a double-blind manner. Data were presented as means ± SEM unless stated. The statistical analyses were performed using Prism 6 (GraphPad Software, USA) and MATLAB 2013b (MathWorks, USA). Two-tailed paired *t*-test, unpaired *t*-test, one-way or two-way ANOVA with *post hoc* Bonferroni test were used. The cutoff for significance was held at $P = 0.05$.